Revisiting the linear forcing of turbulence in single-phase and two-phase flows

Victor Boniou, Stéphane Jay, Guillaume Vinay, Jean-Lou Pierson

Revisiting the linear forcing of turbulence in single-phase and two-phase flows

Victor Boniou and Stéphane Jay
IFP Energies nouvelles, Institut Carnot Transports Energie, 92500 Rueil-Malmaison, France

Guillaume Vinay and Jean-Lou Pierson
IFP Energies nouvelles, Institut Carnot Transports Energie, 69360 Solaize, France

This paper presents a comprehensive framework for addressing the challenges associated with turbulence linear forcing in incompressible single-phase and two-phase flows. By examining existing literature on linear forcing techniques for single-phase flows, which typically yield constant turbulent production, kinetic energy, or dissipation rates, we derive a general method based on constant energetics. This method ensures that any constant power of kinetic energy multiplied by any constant power of dissipation rate remains unchanged over time. A linear stability analysis of this forcing method is performed, demonstrating its relevance and suitability in practical scenarios. Then, a novel solution is proposed for addressing numerical dissipation by measuring and including it in the linear forcing term. This methodology is adapted to the general method proposed for constant energetics and validated on a single-phase flow. Finally, we investigate the linear forcing of turbulence in two-phase flows. Removing the mean contribution of the capillary forces prevents the exponential growth of kinetic energy. The paper also explores the impact of capillary forces on the energetics budgets and their implications for turbulent forcing. The framework is validated through turbulent emulsion and mono-disperse droplet-laden turbulence scenarios, demonstrating its feasibility across various two-phase flow applications.

I. INTRODUCTION

Turbulent multiphase flows are of great interest for numerous applications ranging from environmental processes, such as atmospheric cloud formation [1] and sediment transport [2], to industrial applications like multiphase reactors [3] and fuel injection systems [4]. The numerical simulation of these processes requires properly generating and controlling turbulence in the presence of dispersed phases.

To generate and maintain single-phase turbulence, different approaches have been proposed. The linear forcing method [5] has shown a noticeable gain in interest in the past two decades because, in contrast to spectral methods, it does not require a domain with periodic boundary conditions and may be readily used in variable density simulations [6]. Moreover, it does not require working in the spectral space, avoiding the burden of Fourier transforms, which may lead to additional computational cost when using a non-spectral code [7]. This gain of versatility led to numerous adaptations of the method for rectangular domains or partial forcing in only a portion of the domain with reasonable control of global turbulence quantities in the context of turbulent combustion [8, 9]. In the linear forcing method, a source term linearly proportional to the fluid velocity is introduced into the momentum transport equation, which reads $A\mathbf{u}$. A is the forcing coefficient and $\mathbf{u}$ the fluid velocity. This forcing acts in the physical space as a production term that injects energy at all scales [10] in opposition to spectral methods that may select the wave numbers where turbulence is injected [11]. The pioneering work of Lundgren [5] has been analyzed by Rosales and Meneveau [6], who concluded that the original form suffers from two main limitations:

- The slow convergence to a statistically stationary state and large temporal oscillations around the prescribed values related to turbulence.
- The integral length imposed by the domain size, i.e., at a scale $\ell \approx 0.19\mathcal{L}$ with $\mathcal{L}$ the periodic box length [6].

The issue of statistical convergence can be cured by adjusting the coefficient A that multiplies the velocity. In Carroll and Blanquart [10], the unsteady measure of the turbulent kinetic energy in the box is included in the forcing amplitude. This small addition allows it to converge faster to the prescribed turbulent intensity, even if large oscillations around the expected value are still observed. In Bassenne *et al.* [12], new forms are proposed that can converge rapidly to nearly constant kinetic energy k or dissipation rate ϵ. A hybrid form is also proposed to minimize the oscillation amplitude of k and ϵ. This last approach leads to an excellent trade-off between the control of k and ϵ. Similar forms of A were used in different works to control k [9, 13, 14]. Regarding the control of integral length, several studies propose to filter the velocity present in the force with a diffusion equation [15], a Gaussian kernel [9], a top hat filter [16] or the Raymond & Garder's implicit sine filter [17]. Finally, specific flows have been treated with extensions of Lundgren's linear forcing to anisotropic turbulence [15] and inhomogeneous turbulence [16]. Note that the control of integral length and inhomogeneous anisotropic turbulence is beyond the scope of the paper.

We must investigate several aspects to adapt Lundgren's linear forcing to two-phase flows. The original method relies on a framework where the kinetic energy budget can be easily derived. Its extension to interfacial flows with surface tension must be written and the linear forcing modified accordingly [18]. Moreover, the numerical approximation of Navier-Stokes equations does not always conserve kinetic energy due to the additional challenges of numerically capturing interfaces. The discrete conservation of kinetic energy is not a trivial feature for the numerical approximation of a single-phase flow [19] and is even more challenging to obtain for a two-phase flow employing an interface capturing method [20]. Indeed, most of the two-phase flow solvers of the literature do not fulfill this conservation property [21–25]. Despite its practical importance, a detailed analysis of conservation loss and its consequences on the linear forcing is lacking.

Moreover, while employing Lundgren's forcing, some issues have been observed by Chouippe and Uhlmann [7] for particle-laden flows. In their simulations, the additional forces due to the two-way coupling modify the kinetic energy balance and lead to unbounded growth of the kinetic energy. This issue can be minimized by removing the mean flow in the computation of the forcing term. Other authors argued that the velocity used to force turbulence should not be correlated to the velocity of the flow [7, 13]. Then, an external stochastic process based on velocities randomly generated in the spectral space [11] was used to avoid such exponential growth of kinetic energy. Other external processes based on inherently chaotic velocity fields, such as ABC flows [26] have been successfully employed by Crialesi-Esposito *et al.* [27] to simulate turbulent emulsions. More recently, Yao and Capecelatro [28] propose to remove the mean part of the two-way coupling force while using Lundgren's forcing to retrieve bounded kinetic energy.

Finally, Lundgren's forcing has been revisited by Duret *et al.* [29] to simulate homogeneous isotropic turbulence (HIT) of two-phase flows with phase change using a direct measure of the kinetic energy budget in the periodic box. This approach indirectly considers the additional contributions to the energy budget by a simple measure of kinetic energy change in time. Such a method avoids computing an energy budget, which can be tedious in the context of two-phase flows with phase change.

Following the work of Bassenne *et al.* [12] and Duret *et al.* [29], this paper tackles the issue of forcing homogeneous isotropic turbulence in single-phase and two-phase flows where capillary forces are captured. The reexamination of the state-of-the-art allows us to propose a general form of linear forcing that imposes any constant power of kinetic energy multiplied by any constant power of dissipation rate. We also extend the linear forcing to numerical solvers suffering from numerical dissipation thanks to an indirect measure of the energy budget as proposed by Duret *et al.* [29]. The different numerical experiments performed with the Basilisk solver [21] give general best practices to force turbulence in a two-phase flow, which can also extend to other flow types. The paper is presented as follows. First, the numerical setup used for numerical experiments is presented in section II. Then, the general methodology of Lundgren's linear forcing is described for an incompressible single-phase flow in section III. In section IV, the control of energetics in single-phase flows is introduced with the issue of numerical dissipation evidenced by numerical experiments. This issue is further studied in section V, along with a solution to overcome it. Finally, the linear forcing for two-phase flows is treated by addressing the additional numerical issues in section VI. Section VII presents conclusions and perspectives of this work.

II. NUMERICAL METHODOLOGY

Before delving into the specifics of turbulence forcing, this section introduces the numerical setup employed in this work. For two-phase flows, the incompressible Navier-Stokes equations can be written following the single-field formalism [30]

$$\frac{\partial \alpha}{\partial t} + \nabla \cdot (\alpha \mathbf{u}) = 0, \tag{1}$$

$$\nabla \cdot \mathbf{u} = 0, \tag{2}$$

$$\rho \left(\frac{\partial \mathbf{u}}{\partial t} + \nabla \cdot (\mathbf{u} \otimes \mathbf{u}) \right) = -\nabla p + \nabla \cdot (\mu \nabla \mathbf{u}) + \rho \mathbf{f}_T + \mathbf{f}_\sigma, \tag{3}$$

where α is the volume fraction of the dispersed phase, $\mathbf{u}$ is the fluid velocity, t is the time, p is the fluid pressure, $\mathbf{f}_T$ is the turbulent forcing term which sustains turbulence in the flow. Following the single-field formalism, $\mathbf{f}_\sigma$ is the local density of the capillary force per unit volume, ρ the average density and μ the average viscosity defined as

$$\mathbf{f}_\sigma = \sigma \kappa \nabla \alpha, \quad \rho = \alpha \rho_1 + (1-\alpha)\rho_2, \quad \mu = \alpha \mu_1 + (1-\alpha)\mu_2, \tag{4}$$

with σ the surface tension and κ the mean curvature of the interface. The subscripts refer to phases 1 and 2.
The numerical simulations are performed with the Basilisk solver [21]. The solver uses a second-order order projection

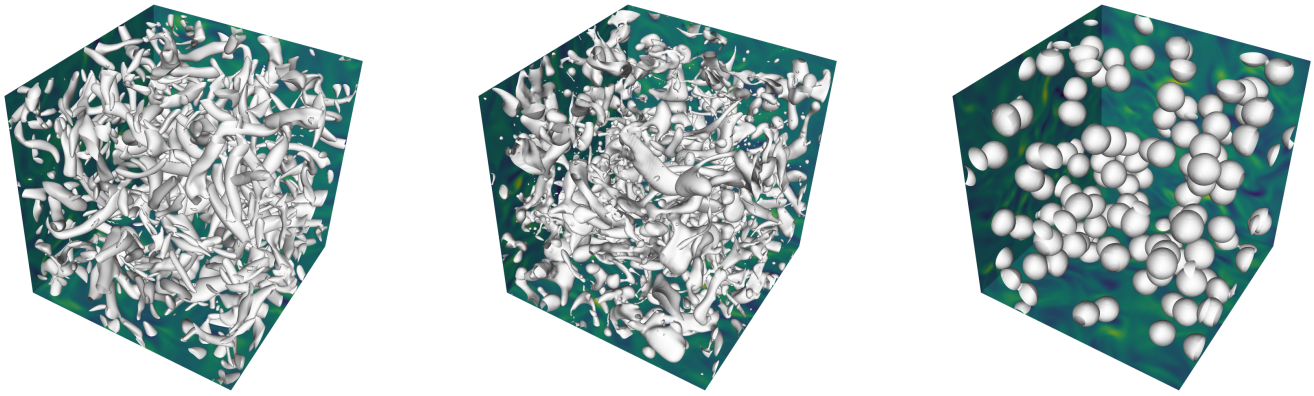

(a) Single-phase HIT (SP) (b) Turbulent emulsion (TPE) (c) Droplet-laden HIT (TPD)

FIG. 1: Illustration of three configurations of interest for the linear forcing of turbulence. (a) : the isocontour $\lambda_2 = -5$ appears in white [35]. (b) and (c) : the interface isocontour $\alpha = 0.5$ appears in white. The vorticity field in x-direction is displayed on the planes.

method in space and time [31] for equations (2) and (3) and an interface capturing method based on the geometric Volume-of-Fluid [32] with a PLIC reconstruction [33]. The interface and the momentum equation are coupled through the capillary force modeled by a well-balanced continuum-surface-force formulation [34] with the curvature estimated from height functions [21].

The numerical setup comprises a triple periodic box with length $\mathcal{L} = 2\pi$, accommodating both single-phase and two-phase flows. Three test cases are considered to encompass relevant applications. They are illustrated in fig. 1 and the main physical and numerical parameters are summed up in table I.

Case	ρ	μ	Re_λ	We	d/η	$\langle\alpha\rangle_\Omega$
SP	1	0.005	40	–	–	–
TPE	1	0.005	40	25	–	0.1
TPD	1	0.005	40	0.5	20	0.1

TABLE I: Physical and numerical setup for the three different cases

First, a single-phase (SP) test case is studied, which aligns with a classic HIT as pictured in fig. 1a. We define the Taylor-microscale Reynolds number as

$$Re_\lambda = \frac{\rho \lambda u_0}{\mu}, \tag{5}$$

where u_0^2 is the variance of the velocity field ($u_0^2 =< u_i u_i >_\Omega /3$) and λ is the Taylor-microscale defined as $\lambda = \sqrt{15\nu u_0^2/\epsilon_0}$ with $\nu = \mu/\rho$ the kinematic viscosity. $\langle \cdot \rangle_\Omega$ denotes spatial averaging over the whole domain and $\epsilon_0 = \langle \nu \nabla \mathbf{u} : \nabla \mathbf{u} \rangle_\Omega$ is the average dissipation rate. The SP test case is initialized with a solution obtained from a prescribed energy spectrum $E_0(\kappa)$ given by eq. (A2), which already has the target kinetic energy k_0 [10]. An important aspect of the linear forcing is worth emphasizing: the initial velocity field should not influence the long-term statistically converged state. We have tested two different ways of initializing the velocity field in Appendix A. Both lead to the same results after a short transient whose duration depends on the prescribed methodology.

A second test case involves an emulsion (TPE) where a wide range of scales is generated through turbulence (see fig. 1b). The TPE test case can be related to various works of the literature from liquid-gas with phase-change [29, 36] to liquid-liquid systems [27, 37]. The density and dynamic viscosity are equal in both phases, and the hold-up is taken as $\langle\alpha\rangle_\Omega = 0.1$. The initial solution consists of the steady state of the SP test case for the velocity field and a single spherical droplet of diameter d such that the Weber number $We = 0.5\rho u_0^2 \mathcal{L}/\sigma = 25$ as in [38].

Finally, a third test case is considered corresponding to a droplet-laden HIT (TPD) with a monodisperse distribution as illustrated in fig. 1c. The TPD test case is analogous to the study of finite-size particles interacting with turbulence [28, 39, 40]. As for the TPE test case, the density and dynamic viscosity are taken equal in both phases, and the volume fraction is taken as $\phi = 0.1$. The Weber number $We = 2\rho\epsilon_0^{2/3} d^{5/3}/\sigma = 0.5$ with the droplet diameter $d = 20\eta$ ensures that the droplet cannot break up according to the Hinze-Kolmogorov theory [41]. An additional treatment

is used for the TPD case to avoid coalescence, which ensures that the droplet population remains monodisperse. This method relies on a multi-VOF representation of the interface [42, 43], which transports different VOF fields for droplets when they are too close to each other. Then, no coalescence occurs due to the presence of two interfaces in the same cell, as it happens using a standard VOF-PLIC method. However, this method can be quite expensive as it requires solving a transport equation for each VOF field. To avoid this issue, an algorithm called `no-coalescence.h` is implemented. More details on this algorithm can be found in a manuscript in preparation [43]. The choice of a small Weber number and the use of the multi-VOF method allows for keeping a single-size droplet population in the presence of turbulence.

If not specified, all simulations are conducted with $N_x = 256$ cells per direction and a prescribed $Re_\lambda = 40$. This choice for the grid resolution leads to $\kappa_{max}\eta > 9$ with $\kappa_{max} = 2\pi/\Delta x$ the highest captured wavenumber. This Reynolds number is relevant to the intended applications involving two-phase flows and minimizes the influence of numerical dissipation discussed in section V. The calculations are performed during an extended period of $T = 100\tau_\ell$, with $\tau_\ell = \ell/u_0$ the integral timescale, to ensure statistical convergence.

III. GENERAL PHILOSOPHY OF LUNDGREN'S LINEAR FORCING

First, we present the pioneering work of Lundgren [5] in the context of incompressible flows. In the case of a single-phase incompressible flow, eqs. (2) and (3) yield

$$\nabla \cdot \mathbf{u} = 0, \tag{6}$$

$$\rho\left(\frac{\partial \mathbf{u}}{\partial t} + \nabla \cdot (\mathbf{u} \otimes \mathbf{u})\right) = -\nabla p + \mu \nabla^2 \mathbf{u} + \rho \mathbf{f}_T, \tag{7}$$

In the generic framework of HIT, where the domain consists of a triple-periodic box, the total kinetic energy budget can be established by taking the scalar product of eq. (7) by $\mathbf{u}$ and spatial averaging $\langle \cdot \rangle_\Omega$ over the whole domain [44]. This yields,

$$\frac{\partial k}{\partial t} = -\epsilon + \mathcal{P}_T, \tag{8}$$

where $k(t)$ is the volume averaged kinetic energy, $\epsilon(t)$ is the volume averaged dissipation rate, $\mathcal{P}_T(t)$ the volume averaged turbulent production through forcing. k, ϵ and $\mathcal{P}_T$ may be expressed as

$$k = \frac{1}{2}\langle \mathbf{u} \cdot \mathbf{u} \rangle_\Omega, \quad \epsilon = \langle \nu \nabla \mathbf{u} : \nabla \mathbf{u} \rangle_\Omega, \quad \mathcal{P}_T = \langle \mathbf{f}_T \cdot \mathbf{u} \rangle_\Omega. \tag{9}$$

The linear turbulent forcing term may be defined as

$$\mathbf{f}_T = A(\mathbf{x}, t)\mathbf{u}. \tag{10}$$

In Lundgren [5] original work, A is kept constant in space and time such that $A(\mathbf{x}, t) \equiv A_0$. At steady state eq. (8) reduces to

$$\epsilon_0 = 2A_0 k_0, \tag{11}$$

which leads to $A_0 = \epsilon_0/(2k_0)$ where the subscript 0 refers to the steady state (target) turbulent quantities. The knowledge of the integral length scale $\ell = (u_0^2)^{3/2}/\epsilon_0$ and the variance of the velocity field u_0^2 lead to all other turbulent quantities:

$$Re_\lambda = \left(\frac{15u_0\ell}{\nu}\right)^{\frac{1}{2}}, \quad k_0 = \frac{3}{2}u_0^2, \quad \epsilon_0 = \frac{u_0^3}{\ell}, \quad \tau_\ell = \frac{3\ell}{2u_0}, \quad A_0 = \frac{u_0}{3\ell}. \tag{12}$$

Using eq. (11), Carroll and Blanquart [10] define the turbulent quantities in terms of ℓ and A_0

$$Re_\lambda = \left(\frac{45A_0\ell^2}{\nu}\right)^{\frac{1}{2}}, \quad k_0 = \frac{27}{2}A_0^2\ell^2, \quad \epsilon_0 = 27A_0^3\ell^2, \quad \tau_\ell = \frac{1}{2A_0}, \quad u_0 = 3A_0\ell. \tag{13}$$

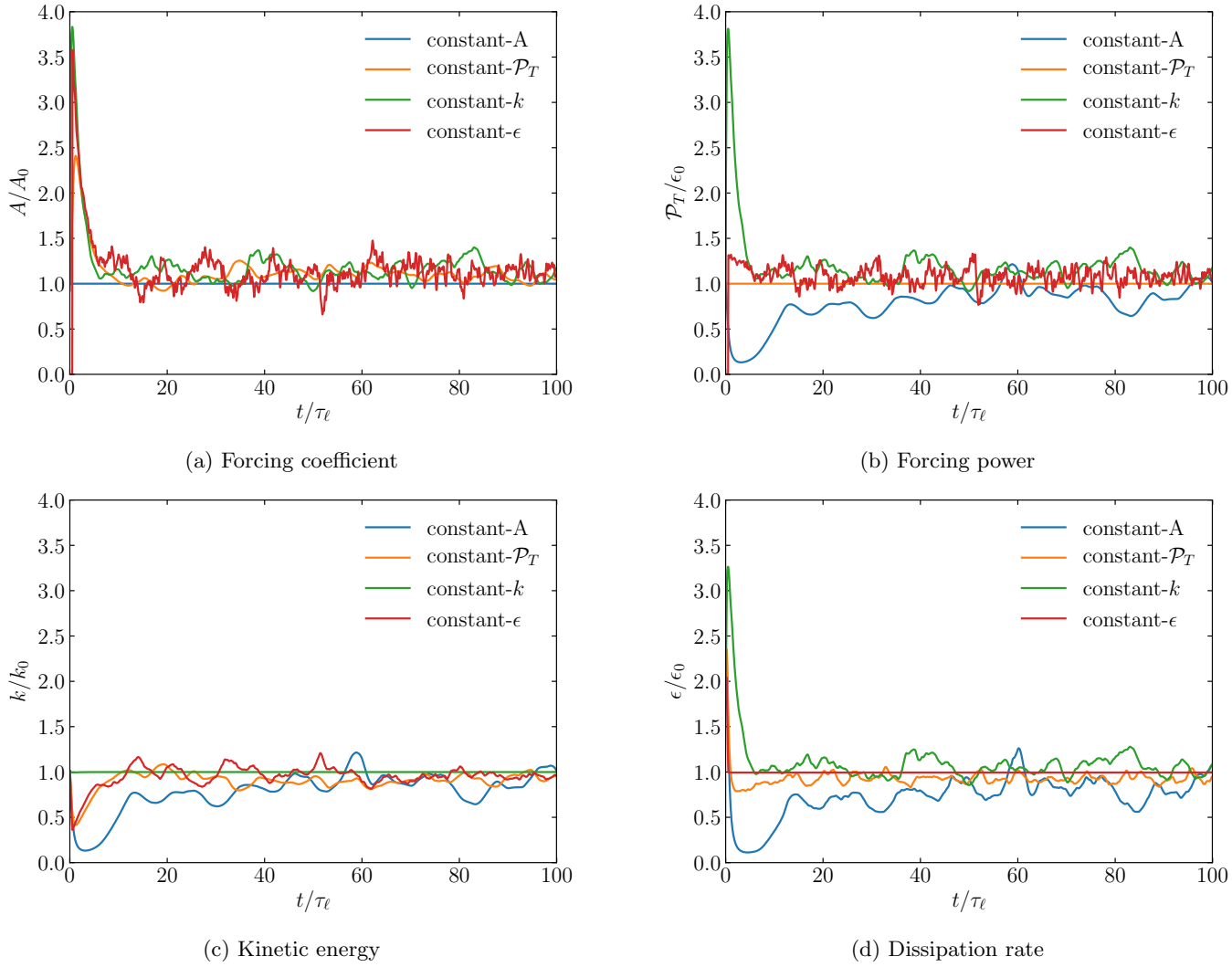

(a) Forcing coefficient

(b) Forcing power

(c) Kinetic energy

(d) Dissipation rate

FIG. 2: Time evolution of various quantities using different forcing methods for SP test case. (a): evolution of the forcing coefficient A, (b): evolution of the turbulent production $\mathcal{P}_T$, (c): evolution of the kinetic energy k, (d): evolution of the dissipation rate ϵ. The constant-A forcing refers to the original method of Lundgren [5] defined by eq. (10) with $A = A_0$, the constant-$\mathcal{P}_T$ refers to the method of Carroll and Blanquart [10] defined by eq. (14), the constant-k and constant-ϵ refer to the methods of Bassenne *et al.* [12] defined by eqs. (19) and (23) respectively with $\tau_k = \tau_\epsilon = \tau_\ell/67$.

IV. MODIFICATION OF THE ORIGINAL LINEAR FORCING APPROACH

The study conducted by Rosales and Meneveau [6] revealed that the pioneering work of Lundgren converges slowly to the prescribed turbulent kinetic energy. Moreover, the solution exhibits large temporal oscillations around the prescribed values (as shown by the blue line in fig. 2). This feature of the constant-A forcing prevents the acquisition of statistically converged turbulence data when additional physics is considered, such as particle-laden flows [12]. In the following, we present some solutions proposed in the literature to overcome this limitation and better control the energetics in the turbulent flow. The evolution of the forcing amplitude A, forcing power $\mathcal{P}_T$, kinetic energy k, and dissipation rate ϵ are displayed in fig. 2 for the four main methods presented in this section as an illustration of their behavior on the single-phase test case SP. We also propose a general formulation encompassing constant-energetics methods and compare it to the hybrid approach of Bassenne *et al.* [12].

A. Constant turbulent production $\mathcal{P}_T$

In [10], a first attempt to monitor the turbulent kinetic energy k has been proposed where the measure of $k(t)$ in the domain at time t is included in the forcing amplitude

$$A(t) = A_0 \frac{k_0}{k(t)}, \tag{14}$$

where k_0 is the desired kinetic energy and A_0 is the amplitude computed from the prescribed turbulence. Palmore Jr and Desjardins [17] noticed that such a forcing prescribes a constant turbulent production over time matching exactly the target dissipation rate ϵ_0:

$$\mathcal{P}_T = \left\langle A_0 \frac{k_0}{k} \mathbf{u} \cdot \mathbf{u} \right\rangle_\Omega = 2A_0 k_0 = \epsilon_0. \tag{15}$$

This slight modification of Lundgren's initial form allows the solution to converge faster to the prescribed turbulent intensity, even if oscillations around the expected value are still observed. In fig. 2b, it is clear that the turbulent production of this method exactly matches the target dissipation rate ϵ_0 while the kinetic energy and dissipation rate are oscillating around the target values in fig. 2c and fig. 2d respectively.

B. Constant kinetic energy k

In the literature, some authors define a coefficient of the form

$$A(t) = \max\left[\frac{k_0 - k(t)}{\Delta t\, k_0}, 0\right] \tag{16}$$

with Δt the computational timestep. The coefficient A acts as a bang-bang controller, stopping the forcing when the target kinetic energy is reached. The kinetic energy is then dissipated, and the forcing starts again to retrieve the target kinetic energy. More sophisticated forms based on a PID controller [14, 45] can also be used to improve the abrupt changes in forcing amplitude displayed by eq. (16).

Another strategy is presented by Bassenne *et al.* [12] to properly derive a constant-k forcing coefficient from the kinetic energy budget. By noticing that Lundgren's form of turbulent production writes $2Ak$, eq. (8) becomes:

$$\frac{\partial k}{\partial t} = -\epsilon + 2Ak. \tag{17}$$

In the original work of Lundgren [5], the strong hypothesis of instantaneous steady state $\partial k/\partial t = 0$ was invoked and can be softened by a relaxation of the form:

$$\frac{\partial k}{\partial t} = -\frac{k - k_0}{\tau_k}, \tag{18}$$

with τ_k the timescale of relaxation to the prescribed kinetic energy k_0 from the actual kinetic energy k. Combining eqs. (17) and (18) and rearranging the terms lead to the new forcing coefficient:

$$A(t) = \frac{k_0 - k(t)}{2\tau_k k(t)} + \frac{\epsilon(t)}{2k(t)}. \tag{19}$$

It was found by Bassenne *et al.* [12] that the relaxation time τ_k should be smaller than τ_ℓ to ensure small temporal oscillations around the target turbulence. In this work, this relaxation time is set to $\tau_k = \tau_\ell/67$ as proposed in [12]. It is clear from fig. 2c that this method is able to prescribe the target kinetic energy k_0, which remains constant in time. However, the dissipation rate experiences oscillations around the prescribed value as demonstrated in fig. 2d.

C. Constant dissipation rate ϵ

A forcing coefficient was also derived by Bassenne *et al.* [12] to impose a constant dissipation rate ϵ. First, the transport of ϵ is obtained by differentiating eq. (7) with respect to $\mathbf{x}$ and multiplying it by $2\nu\nabla\mathbf{u}$:

$$\frac{\partial \epsilon}{\partial t} = -\vartheta + 2A\epsilon, \tag{20}$$

where ϑ is the term of production and dissipation of ϵ which may be expressed as (with Einstein notation):

$$\vartheta = 2\left\langle \nu \frac{\partial u_i}{\partial x_k}\frac{\partial u_j}{\partial x_k}\frac{\partial u_i}{\partial x_j}\right\rangle + 2\left\langle \nu^2 \frac{\partial}{\partial x_j}\left(\frac{\partial u_i}{\partial x_k}\right)\frac{\partial}{\partial x_j}\left(\frac{\partial u_i}{\partial x_k}\right)\right\rangle. \tag{21}$$

By allowing ϵ to relax to the prescribed value ϵ_0:

$$\frac{\partial \epsilon}{\partial t} = -\frac{\epsilon - \epsilon_0}{\tau_\epsilon}, \tag{22}$$

the constant-ϵ form is derived:

$$A(t) = \frac{\epsilon_0 - \epsilon(t)}{2\tau_\epsilon \epsilon(t)} + \frac{\vartheta(t)}{2\epsilon(t)}. \tag{23}$$

As for the constant-k form, τ_ϵ must be small compared to τ_ℓ and is set to $\tau_\epsilon = \tau_k = \tau_\ell/67$ in this work. As depicted in fig. 2d, the method is able to prescribe the target dissipation rate ϵ_0 while k is oscillating around the target value k_0 in fig. 2c. The turbulent production shows oscillations with the highest frequency in fig. 2b, which reflects stronger temporal variations of the higher-order energetics ϵ compared to k.

D. A general framework for constant-energetics linear forcing

While k and ϵ are the usual quantities of interest to characterize a turbulent flow, other turbulent quantities can be written in terms of k and ϵ:

$$\ell \sim \frac{k^{\frac{3}{2}}}{\epsilon}, \quad \tau_\ell \sim \frac{k}{\epsilon}, \quad Re_\lambda \sim \frac{k}{\epsilon^{\frac{1}{2}}}. \tag{24}$$

Let us define a general turbulent quantity $\Phi \sim k^a \epsilon^b$ and write its time derivative:

$$\frac{1}{\Phi}\frac{\partial \Phi}{\partial t} = \frac{a}{k}\frac{\partial k}{\partial t} + \frac{b}{\epsilon}\frac{\partial \epsilon}{\partial t}. \tag{25}$$

By using eqs. (17) and (20), eq. (25) becomes:

$$\frac{a}{k}\frac{\partial k}{\partial t} + \frac{b}{\epsilon}\frac{\partial \epsilon}{\partial t} = \frac{a}{k}\left(-\epsilon + 2Ak\right) + \frac{b}{\epsilon}\left(-\vartheta + 2A\epsilon\right). \tag{26}$$

Finally, by substituting eqs. (18) and (22) in eq. (26) and rearranging the terms, a general forcing coefficient can be written as:

$$A(t) = \chi\left(\frac{k_0 - k(t)}{2\tau_k k(t)} + \frac{\epsilon(t)}{2k(t)}\right) + (1-\chi)\left(\frac{\epsilon_0 - \epsilon(t)}{2\tau_\epsilon \epsilon(t)} + \frac{\vartheta(t)}{2\epsilon(t)}\right), \tag{27}$$

with the control weight $\chi = a/(a+b)$.

This final form eq. (27) is a generalization of the hybrid approach proposed by Bassenne *et al.* [12] which minimizes the error of eqs. (19) and (23) by a least-square regression. Their formula reads

$$\begin{aligned} A(t) = &\frac{4k^2(t)}{4k^2(t) + 9\tau_{\ell,0}^2\epsilon^2(t)}\left(\frac{k_0 - k(t)}{2\tau_k k(t)} + \frac{\epsilon(t)}{2k(t)}\right) \\ &+ \frac{9\tau_{\ell,0}^2\epsilon^2(t)}{4k^2(t) + 9\tau_{\ell,0}^2\epsilon^2(t)}\left(\frac{\epsilon_0 - \epsilon(t)}{2\tau_\epsilon \epsilon(t)} + \frac{\vartheta(t)}{2\epsilon(t)}\right). \end{aligned} \tag{28}$$

By identification in eqs. (27) and (28), it yields:

$$\chi(t) = \frac{4k^2(t)}{4k^2(t) + 9\tau_{\ell,0}^2\epsilon^2(t)}. \tag{29}$$

Hence, the hybrid approach proposed by Bassenne *et al.* [12] is an alternative form of the general forcing coefficient with χ varying in time to adjust the forcing coming from an error on k or on ϵ. At the steady state $k(t) = k_0$ and $\epsilon(t) = \epsilon_0$, then eq. (29) gives $\chi = 1/2$ which corresponds to the general forcing coefficient with $[a, b] = [1, 1]$.

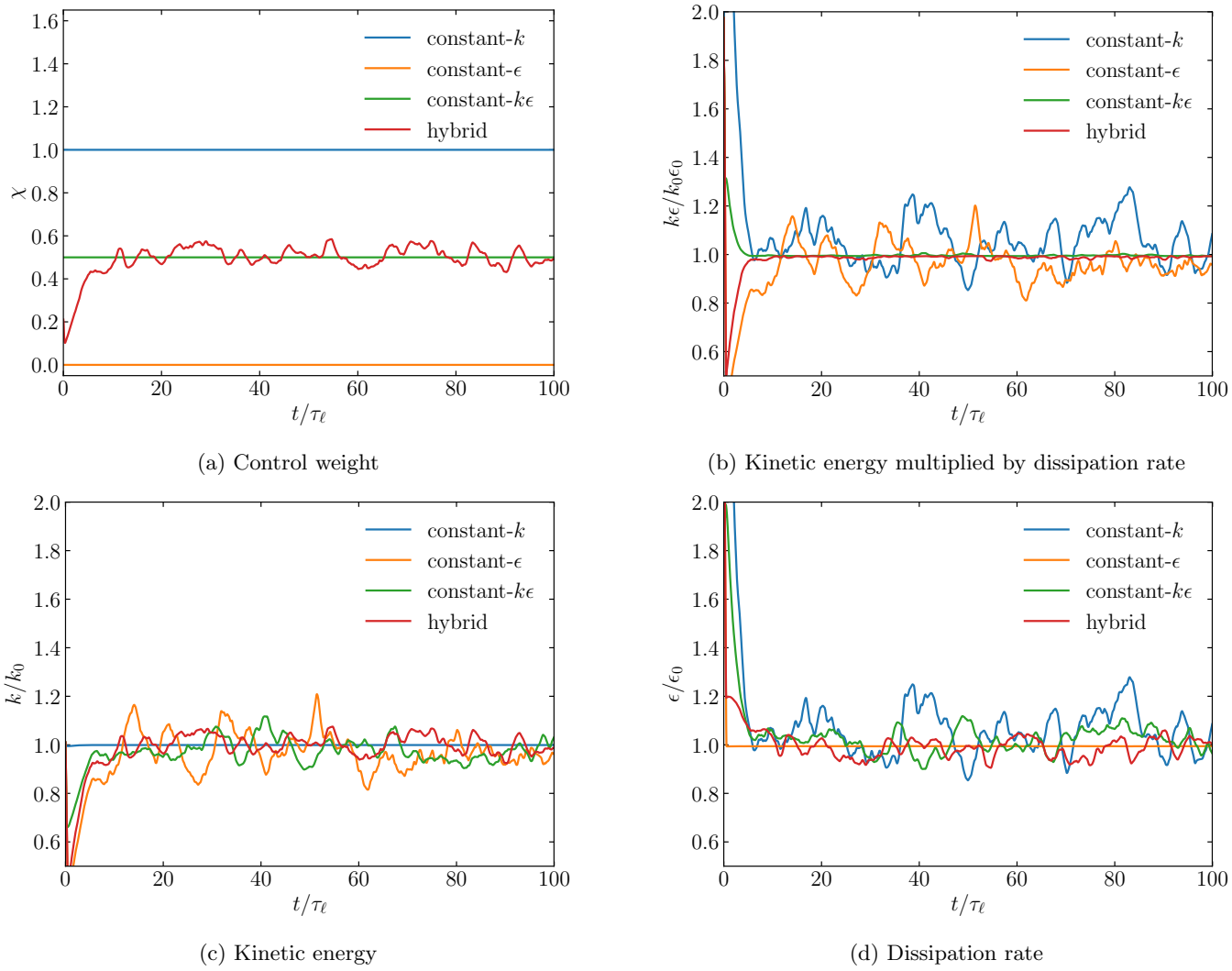

(a) Control weight

(b) Kinetic energy multiplied by dissipation rate

(c) Kinetic energy

(d) Dissipation rate

FIG. 3: Evolution of the control weight χ (a), the kinetic energy multiplied by the dissipation rate $k\epsilon$ (b), the kinetic energy k (c) and the dissipation rate ϵ (d) using different forcing methods for SP test case. The constant-k and ϵ refers to the method of Bassenne *et al.* [12] defined by eqs. (19) and (23) respectively, constant-$k\epsilon$ refers to eq. (27) and hybrid to eq. (28) with $\tau_k = \tau_\epsilon = \tau_\ell/67$.

In fig. 3, the evolution of χ, $k\epsilon$, k and ϵ is provided for constant-k, constant-ϵ, constant-$k\epsilon$ method and the hybrid method of Bassenne *et al.* [12]. All constant-energetics can be related to eq. (27) with different choices of χ. In fig. 3a, constant-k and constant-ϵ methods correspond to $\chi = 1$ and $\chi = 0$ respectively, while constant-$k\epsilon$ corresponds to $\chi = 0.5$ and finally, the value of χ in the hybrid method oscillates around 0.5. There is a short transition regime from the initial solution where the control weight χ is close to zero because the error is the largest for the dissipation rate. The modulation of χ helps the hybrid method to converge faster to the prescribed ϵ_0 compared to the constant-$k\epsilon$ method as depicted in fig. 3d. After this small, unsteady regime, both methods are substantially equivalent. The quantity $k\epsilon$ is shown in fig. 3b to demonstrate the capacity of the proposed general method to prescribe any turbulent quantity by modifying a and b. The hybrid method shows approximately the same behavior as the control weight χ oscillates around the value 0.5 corresponding to a constant $k\epsilon$. Finally, the evolution of k and ϵ, given in figs. 3c and 3d respectively, show that a general approach that combines constant-k and ϵ methods is able to mitigate oscillation amplitudes around both quantities.

This numerical experiment then assesses the proposed general framework, which encompasses all methods of the literature and has the same benefits as the hybrid approach proposed by Bassenne *et al.* [12]. We have also demonstrated that the derivation was consistent with the numerical results: given a couple a and b, the quantity $k^a\epsilon^b$ is controlled and remains constant during the whole simulation. In the present study, $a = b = 1$ leads to $\chi = 0.5$ and a

constant-$k\epsilon$ method. Note that the choice of χ is constrained by the linear stability of the method which is described in the next section.

E. Stability analysis of the methods

In Carroll and Blanquart [10], the linear stability of the constant-A and constant-$\mathcal{P}_T$ methods are performed to provide an explanation for the improvement of the forcing using their modified form. Here, we propose to apply the same procedure to the general constant-energetics forcing method proposed in this paper. This linear stability analysis is based on the hypothesis that the term ϑ in the dissipation rate transport equation can be expressed as in the standard $k-\epsilon$ model

$$\vartheta = \xi \frac{\epsilon^2}{k}, \tag{30}$$

with ξ a positive constant which is close to one [46]. Then, k and ϵ are defined in terms of their asymptotic value k_0 and ϵ_0 and a small perturbation around this value k' and ϵ' such that $k = k_0 + k'$ and $\epsilon = \epsilon_0 + \epsilon'$. By inserting these perturbed forms in eq. (17), the ODE for k' and ϵ' can be found:

$$\frac{\partial k'}{\partial t} = -\frac{k'}{\tau_k}, \tag{31a}$$

$$\frac{\partial \epsilon'}{\partial t} = k' \left(\frac{\xi}{\tau_\ell^2} - \frac{1}{\tau_\ell^2} - \frac{1}{\tau_\ell \tau_k} \right) + \epsilon' \left(\frac{2}{\tau_\ell} - \frac{2\xi}{\tau_\ell} \right), \tag{31b}$$

Note that the Taylor expansions $1/(k_0+k') = 1/k_0 - k'/k_0^2$ and $1/(\epsilon_0+\epsilon') = 1/\epsilon_0 - \epsilon'/\epsilon_0^2$ have been used to derive these expressions. The same procedure can be applied to eq. (20) and gives

$$\frac{\partial k'}{\partial t} = \epsilon' \left(\xi \frac{\epsilon_0}{\tau_\ell} - \frac{\epsilon_0}{\tau_0} \right), \tag{32a}$$

$$\frac{\partial \epsilon'}{\partial t} = \epsilon' \left(\frac{2\xi}{\tau_\ell} - \frac{2}{\tau_\ell} - \frac{1}{\tau_\epsilon} \right). \tag{32b}$$

By assuming that $\xi = 1$, we can find an asymptotic state. The implications of this choice are discussed by Carroll and Blanquart [10], which states that the following analysis cannot be universal for all initial conditions. However, it allows to prove an asymptotic state if the initial solution is close to k_0 and ϵ_0. The final systems for eqs. (31) and (32) can then be written as

$$\frac{\partial}{\partial t} \begin{bmatrix} k' \\ \epsilon' \end{bmatrix} = \frac{1}{\tau_k} \begin{bmatrix} -1 & 0 \\ -\frac{1}{\tau_\ell} & 0 \end{bmatrix} \begin{bmatrix} k' \\ \epsilon' \end{bmatrix} \tag{33}$$

$$\frac{\partial}{\partial t} \begin{bmatrix} k' \\ \epsilon' \end{bmatrix} = \frac{1}{\tau_\epsilon} \begin{bmatrix} 0 & -\tau_\ell \\ 0 & -1 \end{bmatrix} \begin{bmatrix} k' \\ \epsilon' \end{bmatrix}. \tag{34}$$

The first eigenvalue of eqs. (33) and (34) is $\lambda_1 = -1/\tau_k$ and $-1/\tau_\epsilon$ respectively while $\lambda_2 = 0$. The only non-zero eigenvalues from stability analysis are negative, leading to stable systems. The same conclusion was obtained by Carroll and Blanquart [10] for the constant-$\mathcal{P}_T$ with $\lambda_1 = -1/\tau_\ell$ and $\lambda_2 = 0$ while the original Lundgren's form had two zero eigenvalues leading to undamped oscillations. The new feature brought by the constant-k and constant-ϵ methods is controlling the time to dampen the perturbation by τ_k and τ_ϵ. In the case of constant-$\mathcal{P}_T$, this time is inherently set to τ_ℓ. The effect of the choice of τ_k or τ_ϵ has been studied by Bassenne *et al.* [12] leading to the conclusion that the damp time should be smaller than τ_ℓ to obtain a reasonable control of the turbulent quantities.

Now we consider the stability of the general form eq. (27). It can be written as a linear combination of the two above systems eqs. (33) and (34):

$$\frac{\partial}{\partial t} \begin{bmatrix} k' \\ \epsilon' \end{bmatrix} = \begin{bmatrix} -\frac{\chi}{\tau_k} & -\frac{(1-\chi)\tau_\ell}{\tau_\epsilon} \\ -\frac{\chi}{\tau_k \tau_\ell} & -\frac{1-\chi}{\tau_\epsilon} \end{bmatrix} \begin{bmatrix} k' \\ \epsilon' \end{bmatrix}. \tag{35}$$

The eigenvalues of this system are then $\lambda_1 = -\chi/\tau_k - (1-\chi)/\tau_\epsilon$ and $\lambda_2 = 0$. Regardless of the values of τ_k and τ_ϵ, the first eigenvalue λ_1 is negative as long as $\chi > 0$. If $\chi < 0$, λ_1 can become positive depending on the amplitude of τ_k and τ_ϵ. In practice, a and b are taken positive to ensure $\chi > 0$ and $\tau_k = \tau_\epsilon$. These choices do not allow to force turbulent quantities such as Re_λ or τ_ℓ as they usually imply a negative a or b coefficient as presented in eq. (24).

V. IMPACT OF NUMERICAL APPROXIMATION ON THE LINEAR FORCING

The previous section's main focus was on reducing oscillations around the target quantities. However, the mean value of the turbulent quantities at the steady state has yet to be discussed.

Method	k_{mean}/k_0	k_{std}/k_0	$\Delta k_{max}/\epsilon_0$	$\epsilon_{mean}/\epsilon_0$	$\epsilon_{std}/\epsilon_0$	$\Delta\epsilon_{max}/\epsilon_0$
constant-A from eq. (10)	0.897	0.1245	0.3560	0.831	0.1349	0.4402
constant-$\mathcal{P}_T$ from eq. (14)	0.912	0.0487	0.1882	0.927	0.0439	0.1627
constant-k from eq. (19)	0.999	0.0001	0.0012	1.055	0.0877	0.2787
constant-ϵ from eq. (23)	0.962	0.0614	0.2087	0.994	0.0002	0.0063
constant-$k\epsilon$ from eq. (27)	0.971	0.0374	0.0962	1.027	0.0406	0.1096

TABLE II: Mean, standard deviation and maximum oscillation amplitude of k and ϵ with respect to the linear forcing method for SP test case taken from $t/\tau_\ell = 50$ to $t/\tau_\ell = 100$.

In table II, the mean and standard deviation of k and ϵ are reported for t/τ_ℓ ranging from 50 to 100 to remove the transient part. It shows that the only method to prescribe the target kinetic energy k_0 is the constant-k forcing while it oscillates around a lower value for other linear forcing. While Lundgren's forcing underpredicts k and ϵ with 10% error, Carroll's forcing drastically improves the control of k and ϵ with an error below 10% and lower oscillation amplitudes. Finally, the constant-ϵ improves further the control of k even if it is still underpredicted by 4%. These observations were not made in the corresponding references[5, 10, 12] where the kinetic energy and dissipation rate were oscillating around the target values as expected. All these works are based on Numerical Gradient Adaptative (NGA) [19], a solver where the numerical approximation of the Navier-Stokes equations has been constructed to conserve kinetic energy discretely. As detailed in section II, this work relies on the Basilisk solver [21], which employs a second-order finite-volume method that showcases numerical dissipation as presented later. Hence, it will be demonstrated in this section that the discrepancy between the expected results of the literature and the results shown in fig. 2 are caused by the properties of the numerical scheme employed to solve the Navier-Stokes equations.

To the authors' knowledge, the impact of numerical approximation of the Navier-Stokes equations has never been discussed in the context of turbulence forcing. While kinetic energy conservation has been obtained for two-phase flows [20], it is not generally the case in the two-phase flow community [47]. When a contrast in density appears, the conservation of momentum is not trivial to obtain for a two-phase flow solver coupled with Level-Set or VOF methods because of the lack of consistency between the transport of the mass and the momentum [48, 49]. Hence, the conservation of kinetic energy is also lost. Then, the numerical dissipation appears as an additional energy sink in the kinetic energy budget eq. (17):

$$\frac{\partial k}{\partial t} = -\epsilon - \epsilon_{num} + 2Ak, \tag{36}$$

with ϵ_{num} the energy dissipation due to the numerical approximation.

A. An indirect measure of numerical dissipation

The evaluation of ϵ_{num} can be done by quantifying the loss of kinetic energy with time in the simulation and comparing it to the original RHS of eq. (17). For a second-order approximation of the time derivative $\partial k/\partial t$, the central difference could be used as proposed by Schranner *et al.* [50] to measure a posteriori the numerical dissipation on a wide range of simulations. Unfortunately, this discretization cannot be used when numerical dissipation needs to be evaluated on the fly during a simulation because it invokes k at the next time step. In this work, the numerical dissipation is evaluated as follows

$$\epsilon_{num} = -\frac{k^n - k^{n-1}}{\Delta t} - \epsilon^n + 2A^{n-1}k^{n-1}. \tag{37}$$

Following this procedure, it is then possible to quantify the numerical dissipation of the simulations performed above. In fig. 4a, the kinetic energy budget is provided for the SP test case using the constant-k method. It can be observed that the turbulent production $\mathcal{P}_T$ is always higher than the dissipation rate ϵ to compensate the numerical dissipation ϵ_{num} which maintains dk/dt to zero. In fig. 4b, the evolution of ϵ_{num} for different mesh sizes is also reported to ensure that it correctly decreases with increasing resolution.

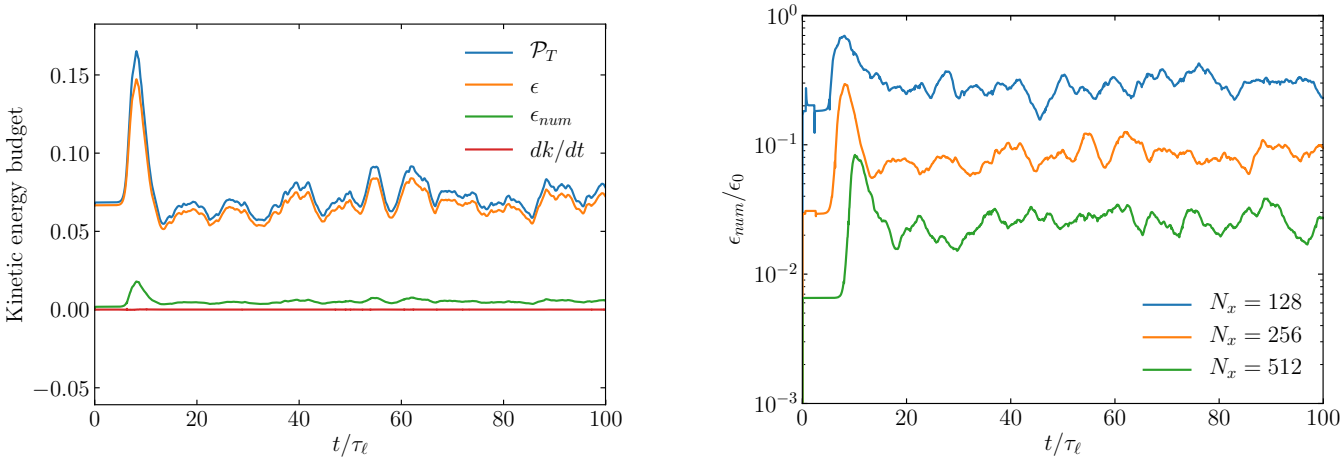

(a) Kinetic energy budget

(b) Numerical dissipation with respect to N_x

FIG. 4: Kinetic energy budget for the mesh $N_x = 256$ (a) and numerical dissipation for different mesh sizes (b) for SP test case with constant-k method defined by eq. (19).

Following the same path, eq. (20), the budget for ϵ can also include an additional term to account for numerical dissipation:

$$\frac{\partial \epsilon}{\partial t} = -\vartheta - \vartheta_{num} + 2A\epsilon, \tag{38}$$

with ϑ_{num} a contribution due to numerical dissipation which is measured as

$$\vartheta_{num} = -\frac{\epsilon^n - \epsilon^{n-1}}{\Delta t} - \vartheta^n + 2A^{n-1}\epsilon^{n-1}. \tag{39}$$

This expression will be useful to incorporate numerical dissipation in the constant-ϵ method.

B. Incorporating numerical dissipation into linear forcing techniques

In Large-Eddy Simulations (LES) an additional source term, in the form of a dissipation term, is added to the momentum transport equation to model the effect of turbulence at unresolved subgrid scales. The turbulent forcing then needs to account for this additional dissipation in the kinetic energy budget [12]:

$$\frac{\partial k}{\partial t} = -\epsilon - \epsilon_{SGS} + 2Ak, \tag{40}$$

with ϵ_{SGS} the subgrid-scale dissipation due to unresolved turbulence. The numerical dissipation is analogous to a subgrid-scale dissipation and can be treated in the same way as long as it can be computed a priori by replacing ϵ_{SGS} by ϵ_{num}. Following the work of Bassenne *et al.* [12], the constant-k forcing eq. (19) can be re-expressed as:

$$A(t) = \frac{k_0 - k(t)}{2\tau_k k(t)} + \frac{C_k(t)}{2k(t)}, \tag{41}$$

with $C_k(t) = \epsilon(t) + \epsilon_{num}(t)$ corresponding to the RHS of eq. (36) without forcing. The term $C_k(t)$ is a direct measure of the total dissipation rate $\epsilon_T(t) = \epsilon(t) + \epsilon_{num}(t)$ approximated by:

$$C_k^{n-1} = 2A^{n-1}k^{n-1} - \frac{k^n - k^{n-1}}{\Delta t}. \tag{42}$$

The effect of this small modification of the original constant-k forcing eq. (19) is presented in fig. 5a. Including the numerical dissipation in the forcing gives a better control of k, which exactly matches the target value k_0. In table III, it can also be stated that this modification slightly decreases the error of the mean value of ϵ from 5.5% to 4.9%.

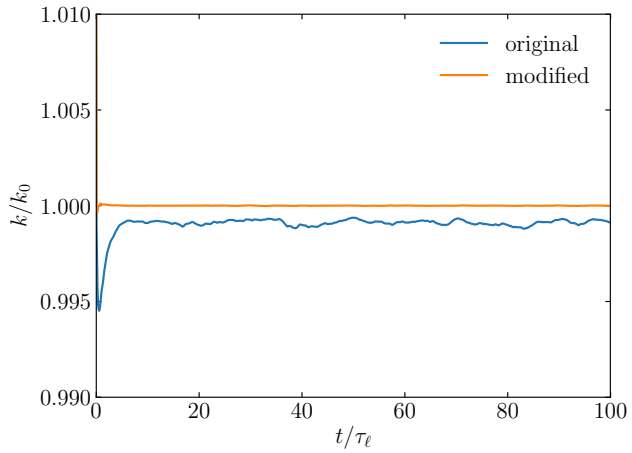

(a) Kinetic energy for constant-k methods

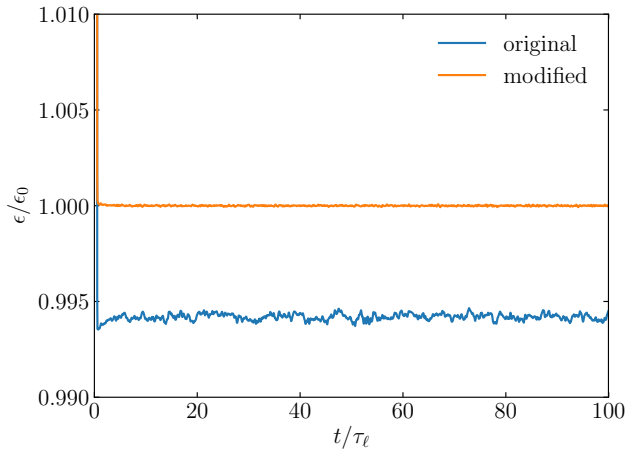

(b) Dissipation rate for constant-ϵ methods

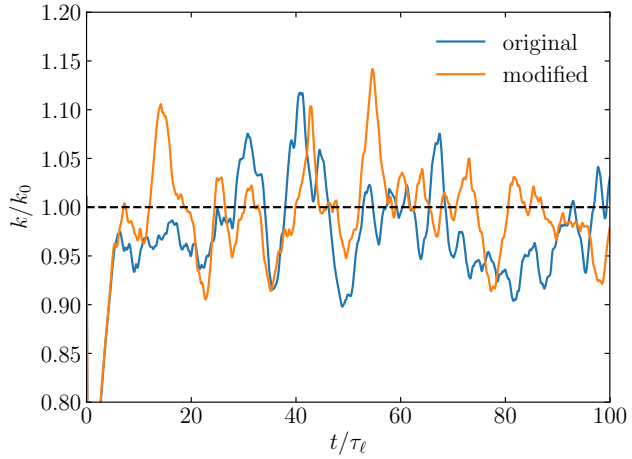

(c) Kinetic energy for constant-$k\epsilon$ methods

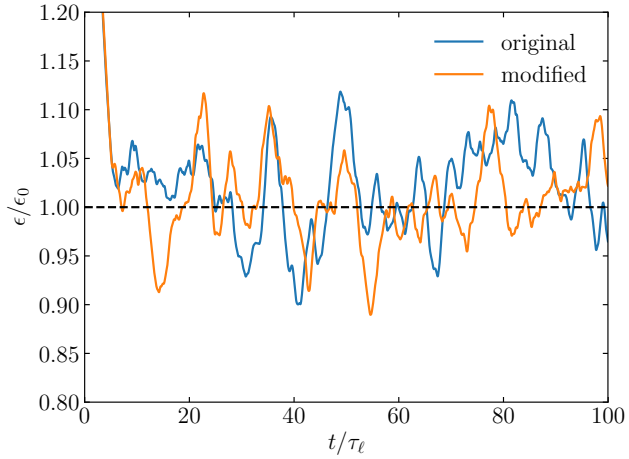

(d) Dissipation rate for constant-$k\epsilon$ methods

FIG. 5: Evolution of k for the original and modified constant-k methods eqs. (19) and (41) respectively (a). Evolution of ϵ for the original and modified constant-ϵ methods eqs. (23) and (46) respectively (b). Evolution of k (c) and ϵ (d) for the the original and modified constant-$k\epsilon$ methods eqs. (27) and (48) respectively.

For a constant-ϵ method, a new budget needs to be written for the total dissipation rate ϵ_T instead of ϵ to follow the work in [12]. The budget for the total dissipation rate is:

$$\frac{\partial \epsilon_T}{\partial t} = -\vartheta_T + 2A\epsilon_T, \tag{43}$$

with $\vartheta_T = \vartheta + \vartheta_{num}$ the dissipation rate of ϵ_T. As for ϵ_{num}, ϑ_{num} needs to be measured at t^{n-1} from

$$\vartheta_T^{n-1} = 2A^{n-1}\epsilon_T^{n-1} - \frac{\epsilon_T^n - \epsilon_T^{n-1}}{\Delta t}. \tag{44}$$

The corresponding constant-ϵ forcing is then:

$$A(t) = \frac{\epsilon_0 - \epsilon_T(t)}{2\tau_\epsilon \epsilon_T(t)} + \frac{\vartheta_T(t)}{2\epsilon_T(t)}. \tag{45}$$

The form eq. (45) has led to unstable results in our numerical experiments. This might be due to the undefined nature of ϵ_{num}, which is not bounded in the case of very strong velocity gradients. Also, it was noted by [12] that the constant-ϵ was not as stable in the LES framework and could depend on initial conditions.

Instead, a stable form is proposed here based on ϵ and C_ϵ the measure of $\vartheta + \vartheta_{num}$:

$$A(t) = \frac{\epsilon_0 - \epsilon(t)}{2\tau_\epsilon \epsilon(t)} + \frac{C_\epsilon}{2\epsilon(t)}, \tag{46}$$

with C_ϵ computed as:

$$C_\epsilon^{n-1} = 2A^{n-1}\epsilon^{n-1} - \frac{\epsilon^n - \epsilon^{n-1}}{\Delta t}. \tag{47}$$

In fig. 5b, the benefits of including the numerical dissipation contribution in the forcing coefficient are exposed. The modified form eq. (46) improves the control of ϵ compared to the original form eq. (23). This is also reported in table III, where the mean value of ϵ matches exactly ϵ_0. At the same time, the mean value of k is also improved with an error of 1.1% compared to 3.8% with the original form. This is at the cost of increasing the standard deviation of k. However, the statistical convergence of both k and ϵ is improved using this method.

Finally, the general forcing method incorporating the numerical dissipation can be retrieved by a linear combination of eqs. (41) and (46):

$$A(t) = \chi \left(\frac{k_0 - k(t)}{2\tau_k k(t)} + \frac{C_k}{2k(t)} \right) + (1-\chi) \left(\frac{\epsilon_0 - \epsilon(t)}{2\tau_\epsilon \epsilon(t)} + \frac{C_\epsilon}{2\epsilon(t)} \right), \tag{48}$$

The consequence of modifying the original constant-$k\epsilon$ method to include numerical dissipation is not so obvious by looking at figs. 5c and 5d. Indeed, both k and ϵ oscillate around the target values by using either the original form eq. (27) or the modified form eq. (48). The outcome of this modification can be showcased by the statistical convergence given in table III. A better statistical convergence of k is observed where the mean value of k obtained from the modified form is 0.2% lower than k_0 compared to 2.9% lower for the original form. The same observation can be done for ϵ which is 0.5% larger than ϵ_0 for the modified form compared to 2.7% for the original form. However, the maximum amplitude and standard deviation are increasing with the modified form. To conclude, the main advantage of using the modified form along with the constant-$k\epsilon$ method is to statistically converge to the prescribed value of k and ϵ simultaneously at the cost of increasing the standard deviation and largest amplitude of the oscillation around k_0 and ϵ_0.

Method	k_{mean}/k_0	k_{std}/k_0	$\Delta k_{max}/\epsilon_0$	$\epsilon_{mean}/\epsilon_0$	$\epsilon_{std}/\epsilon_0$	$\Delta\epsilon_{max}/\epsilon_0$
Original constant-k from eq. (19)	0.999	0.0001	0.0012	1.055	0.0877	0.2787
Modified constant-k from eq. (41)	1.000	0.0000	0.0000	1.049	0.1471	0.3577
Original constant-ϵ from eq. (23)	0.962	0.0614	0.2087	0.994	0.0002	0.0063
Modified constant-ϵ from eq. (46)	0.989	0.0854	0.1924	1.000	0.0000	0.0001
Original constant-$k\epsilon$ from eq. (27)	0.971	0.0374	0.0962	1.027	0.0406	0.1096
Modified constant-$k\epsilon$ from eq. (48)	0.998	0.0408	0.1418	1.005	0.0403	0.1105

TABLE III: Mean, standard deviation and maximum oscillation amplitude of k and ϵ with respect to the linear forcing method for SP test case taken from $t/\tau_\ell = 50$ to $t/\tau_\ell = 100$.

C. Link with the two-phase forcing of Duret et al.

The new form of the constant-k forcing eq. (41) comprising numerical dissipation can be closely related to the form proposed by Duret *et al.* [29] to account for two-phase flow contributions in the kinetic energy budget. Their method avoids computing complex terms related to surface tension and phase change in the kinetic energy budget by indirectly measuring the discrete kinetic energy budget. The term enclosing all other contributions than the turbulent forcing was computed by eq. (42) and the forcing coefficient was retrieved using:

$$A(t) = \frac{k_0 - k(t)}{6\Delta t k(t)} + \frac{C_k(t)}{2k(t)}, \tag{49}$$

which corresponds to eq. (41) with $\tau_k = 3\Delta t$. In this work, $\tau_k = \tau_\epsilon = \tau_\ell/67$ is preferred as it is physically grounded and does not depend on the numerical setup or the mesh.

While the motivation to derive this new form was different in [29], the final idea is the same: additional contributions in the kinetic energy budget are measured when they cannot be computed directly. The new form of the constant-ϵ forcing eq. (46) and the general form given by eq. (48) are then extensions of Duret's method to more general constant-energetics forcings. The next section will show that this strategy is also well-suited for constant-energetics forcing in two-phase flows.

VI. LINEAR FORCING FOR TWO-PHASE FLOWS

In this section, we start by considering the main outcomes encountered when using the schemes derived previously in two-phase flow configurations. Then, using the single-field formalism, we consider the energetic budgets and propose a simple remedy to fix the outcome found in two-phase flow configurations.

A. Exponential growth of kinetic energy

Lundgren's forcing eq. (10) was used by Naso and Prosperetti [51] to study the interaction of a solid particle with turbulence. It was observed that introducing a two-way coupling force in the flow led to a symmetry breaking from numerical sources, leading to $\langle \mathbf{u} \rangle \neq 0$. It was also stated that any mean flow was amplified using the standard linear forcing approach. The same behavior has been observed by Chouippe and Uhlmann [7] in their simulations where the two-way coupling was causing stability issues. In [51, 52], a simple modification of the linear forcing is proposed to minimize this phenomenon:

$$\mathbf{f}_T = A(\mathbf{u} - \langle \mathbf{u} \rangle). \tag{50}$$

By explicitly removing the mean flow, only the fluctuating velocity can be amplified, and the mean flow is no longer affected by the forcing. However, this does not avoid a constant (but not exponential) growth of the mean flow in time, as shown later. In [7, 13], the forcing velocity is randomly generated in the spectral space based on the methodology of Eswaran and Pope [11]. However, it requires working in the spectral space to construct the velocity field, which cancels the main advantage of the linear forcing of working only in the physical space. Other external processes based on inherently chaotic velocity fields such as ABC flows [26] have been successfully employed for the simulation of turbulent emulsions by Crialesi-Esposito *et al.* [27].

Finally, a simple cure to this problem is to remove the mean part of the two-way coupling force. The main argument for this fix is that there is no constraint for the integrated two-way coupling force to be numerically zero in the triply-periodic domain [7]. Then, this force gradually deviates the mean flow to a non-zero value. In [28], the mean part of the two-way coupling force is removed without modifying the philosophy of linear forcing

$$\mathbf{f}_T = A\mathbf{u} - \langle \mathbf{f}_\sigma \rangle \,. \tag{51}$$

For the case of interface capturing methods, the capillary force should sum to zero as it is applied on a set of closed surfaces. However, it is not true at the discrete level using the standard well-balanced discretization for $\mathbf{f}_\sigma$ employed in this work [53]. The discretization of $\mathbf{f}_\sigma$ could make use of the integral formulation instead. In this case, the force can be expressed in a divergence form, which is conservative by nature. A 2D version adapted to the Level-Set method has been proposed by Abu-Al-Saud *et al.* [54], but it remains to be extended to 3D flows and VOF methods and is out of the scope of this paper. Then the linear forcing eq. (51) can be used to prevent the mean flow from taking non-zero values for the present study.

To illustrate this behavior, the mean velocity and the kinetic energy of test cases TPE and TPD are displayed in fig. 6 for the original form eq. (10), the form without mean velocity eq. (50) and the form without mean capillary force eq. (51). The modified constant-k method introduced in section V is used to show that the form of A has no impact on the exponential growth of kinetic energy. The single-phase initialization stage (referred to as SP in fig. 6) illustrates the effect of introducing the dispersed phase on the mean velocity and kinetic energy. For both test cases, the original form of Lundgren leads to an exponential growth of the kinetic energy illustrated here by the growth of the mean x-component of velocity. Removing the mean part of the velocity prevents the exponential growth of the velocity with only a linear growth due to the mean contribution of the capillary force. This is even more clear by comparing the increase of mean velocity for TPE in fig. 6a and for TPD in fig. 6b. Indeed, the magnitude of the growth is higher in the TPE case because of the higher mean capillary force promoted by break-up and coalescence events. The TPD case involves only small deformations of the interface, which are less prone to numerical errors on the capillary force. Finally, when the mean part of the capillary force is removed at each time step, the mean velocity remains bounded close to zero, validating the forcing form of eq. (51) in the scenario of turbulent two-phase flows. This form provides the best results and is employed in the last result section involving two-phase flows.

B. Constant-energetics linear forcing for two-phase flows

The kinetic energy budget for the single-field formulation of Navier-Stokes equations including surface tension reads

$$\frac{\partial k}{\partial t} = -\epsilon + \mathcal{P}_T + \Psi_\sigma, \tag{52}$$

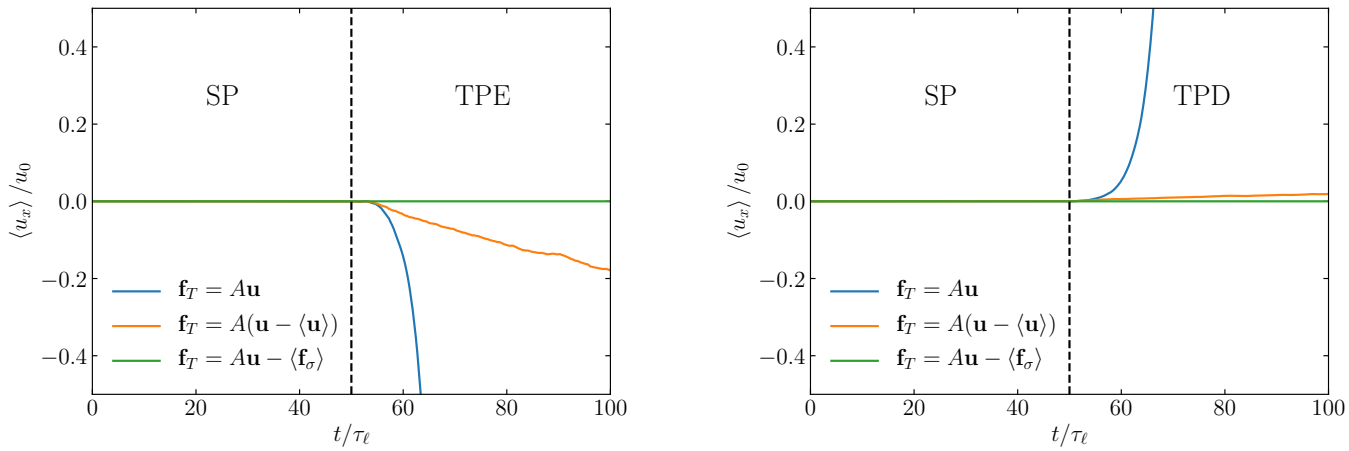

(a) TPE test case

(b) TPD test case

FIG. 6: Mean x-component of velocity in TPE (a) and TPD (b) test cases for the original forcing eq. (10) and the two corrected forms eqs. (50) and (51). Droplets are injected at $t = 50\tau_\ell$.

with Ψ_σ the capillary contribution:

$$\Psi_\sigma = \langle \mathbf{f}_\sigma \cdot \mathbf{u} \rangle \,. \tag{53}$$

In eq. (52), Ψ_σ appears as a sink/source term. Another definition of Ψ_σ is derived from the transport equation of surface tension σ [18]:

$$\Psi_\sigma = -\frac{\sigma}{V_1 \rho_1} \frac{dA}{dt}, \tag{54}$$

with A the total surface of the interface. A third definition can be obtained by summing the kinetic energy budget of each phase [18]. In the following, eq. (53) is used as it is less prone to discrete errors compared to computing numerically the interface area. For the dissipation rate transport, an additional term Φ_σ due to capillary forces arises:

$$\frac{\partial \epsilon}{\partial t} = -\vartheta - \Phi_\sigma + 2A\epsilon, \tag{55}$$

with Φ_σ defined with Einstein summation:

$$\Phi_\sigma = 2 \left\langle \nu \frac{\partial u_i}{\partial x_j} \frac{\partial f_{\sigma,i}}{\partial x_j} \right\rangle . \tag{56}$$

In the previous section, the mean value of the capillary force was discussed with an expected higher deviation to zero for the TPE test case. The capillary contribution in the energy budgets is now studied to provide a complete view of the impact of the two-phase flow on linear forcing. By following the same methodology presented in section IV, the forcing coefficient needs an adjustment to incorporate this additional contribution. Using eq. (52) the constant-k forcing eq. (19) then becomes

$$A(t) = \frac{k_0 - k(t)}{2\tau_k k(t)} + \frac{\epsilon(t)}{2k(t)} - \frac{\Psi_\sigma(t)}{2k(t)}. \tag{57}$$

Thanks to eq. (55) constant-ϵ forcing eq. (23) reads

$$A(t) = \frac{\epsilon_0 - \epsilon(t)}{2\tau_\epsilon \epsilon(t)} + \frac{\vartheta(t)}{2\epsilon(t)} - \frac{\Phi_\sigma(t)}{2\epsilon(t)}. \tag{58}$$

Using the two previous formulations, the general constant-energetics forcing eq. (27) reads

$$A(t) = \chi \left(\frac{k_0 - k(t)}{2\tau_k k(t)} + \frac{\epsilon(t)}{2k(t)} - \frac{\Psi_\sigma(t)}{2k(t)} \right) + (1 - \chi) \left(\frac{\epsilon_0 - \epsilon(t)}{2\tau_\epsilon \epsilon(t)} + \frac{\vartheta(t)}{2\epsilon(t)} - \frac{\Phi_\sigma(t)}{2\epsilon(t)} \right). \tag{59}$$

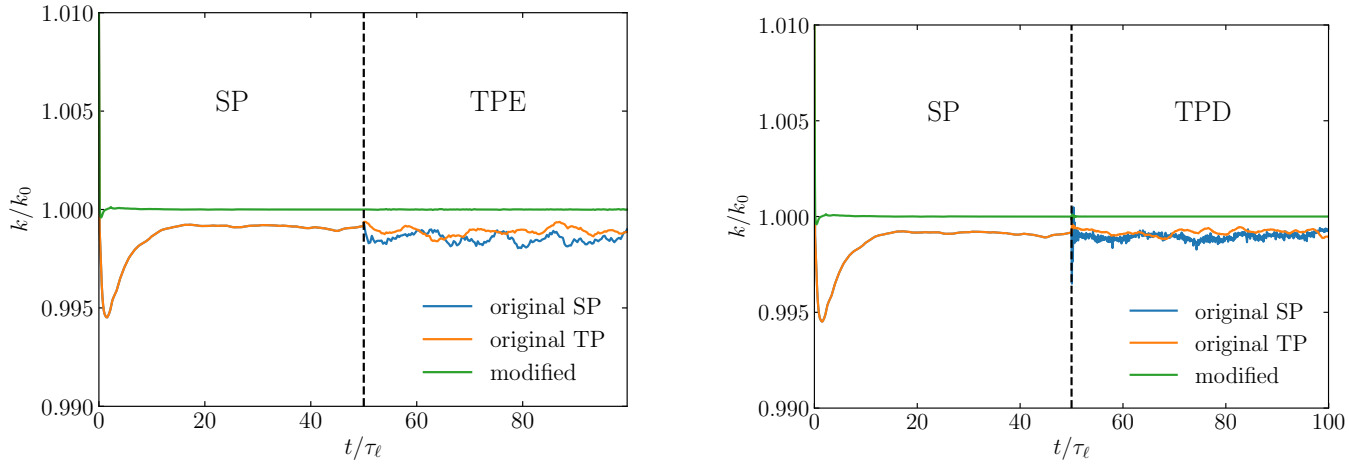

(a) TPE test case

(b) TPD test case

FIG. 7: Evolution of k for the constant-k methods based on original form developed for single-phase flows (original SP) eq. (19), original form extended to two-phase flows (original TP) eq. (57) and modified form eq. (41) with the corrected form of the forcing eq. (51) in TPE (a) and TPD (b) test cases. Droplets are inject at $t = 50\tau_\ell$.

While these forms come from the direct extension of the strategy of Bassenne *et al.* [12], the modified form introduced in section V is expected to also work in the context of two-phase flow without any adjustment. Indeed, the measure of C_k and C_ϵ from eqs. (42) and (47) naturally includes the additional contributions Ψ_σ and Φ_σ.

In fig. 7, the evolution of k for the different forms of constant-k is given in TPE and TPD test cases. The single-phase form eq. (19) remains close to the prescribed value k_0, though it exhibits spurious oscillations around the value. These oscillations are smoothed by employing the two-phase extension eq. (57) even if the kinetic energy is still lower than the target value. Using the form eq. (41) where all terms are comprised in C_k, the kinetic energy is maintained at the target value without any differences with the SP test case. This result shows that the two-phase contribution has little impact on the forcing compared to the numerical dissipation. For the TPE test case, the effect of Ψ_σ is only significant in the transient period where initial break-up occurs [14]. After several eddy-turnover times, a steady state is reached in which break-up and coalescence processes compensate to produce a small quantity Ψ_σ oscillating around zero. Hence, the impact of capillary forces is expected to be negligible in the k budget in most of the cases of interest for capillary-driven flows. For the TPD test case (low Weber number), Ψ_σ is not expected to play a significant role as only small interface deformations will occur. In [18], the magnitude of Ψ_σ is compared to ϵ_0 in decaying turbulence of a droplet-laden flow. It is found that Ψ_σ can only reach a high portion of ϵ_0 (almost 20%) when coalescence occurs while no break-up is observed. In the TPD case, coalescence is prevented numerically, which avoids the situation described in [18]. For other applications, it was found that the two-way coupling contribution was negligible for particles of sizes between 5 and 11 Kolmogorov lengths [40]. The statistical convergence is also provided in tables IV and V where it is clear that the modified form improves the converged state for both k and ϵ. Surprisingly, including the two-phase contribution in the original form leads to a higher difference between ϵ and ϵ_0 with about 10% errors while the original form developed for single-phase flows provides a better convergence for ϵ with less than 1% error. This is not observed in the TPD case where the two-phase contribution is not as predominant.

The extension of the constant-ϵ method to two-phase flow and Duret's forcing is also tested for TPE and TPD test cases. The same observations can be made for the results presented in fig. 8: the single-phase form eq. (23) and two-phase form eq. (58) provide substantially the same results while the form eq. (46) maintains the dissipation rate at the prescribed value ϵ_0. Contrary to the constant-k forcing, the constant-ϵ forcing is more impacted by the two-phase contribution Φ_σ. Indeed, the gap between the target value and the measured value of ϵ is higher when the second phase is injected at $t = 50\tau_\ell$. For the TPE test case, where break-up and coalescence events occur, this gap is above 5%. The two-phase contribution Φ_σ in the ϵ budget has yet to be studied and cannot be compared to previous works. This first result is of great interest from a theoretical perspective and should be continued in future work. By looking at the statistical convergence in tables I and V, the modified form improves the converged state for both k and ϵ.

Finally, the same test cases are performed using the general constant-energetics method. With this approach k and ϵ never fit exactly and oscillate around k_0 and ϵ_0 respectively for the three different RHS computations. Results for TPE and TPD cases are provided in fig. 9. The benefit of the form eq. (48) is less evident than for constant-k and

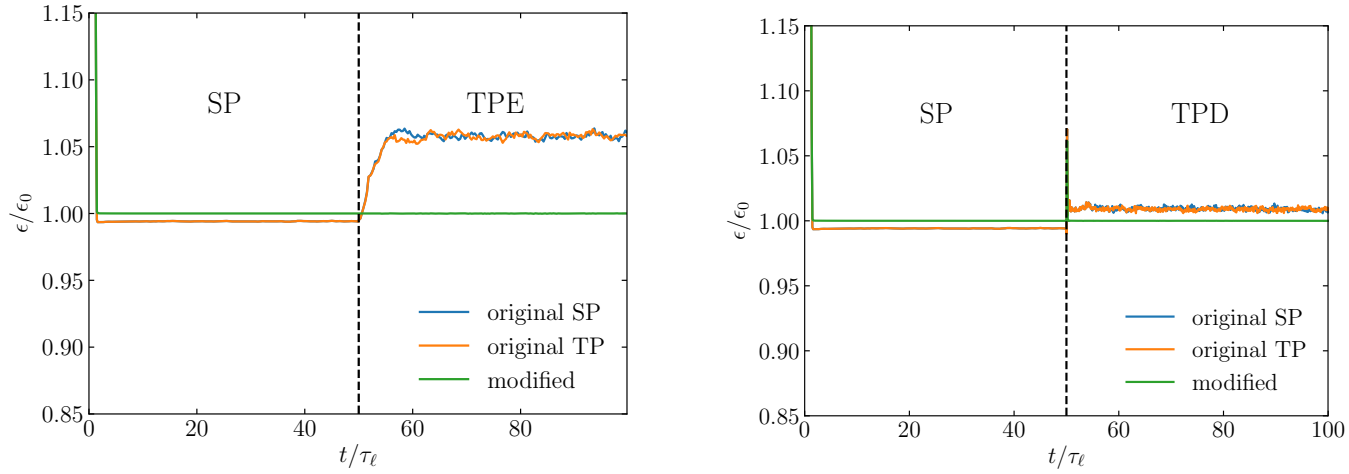

(a) TPE test case

(b) TPD test case

FIG. 8: Evolution of ϵ for the constant-ϵ methods based on the original form developed for single-phase flows (original SP) eq. (23), the original form extended to two-phase flows (original TP) eq. (58) and the modified form eq. (46) with the corrected form of the forcing eq. (51) in TPE (a) and TPD (b) test cases. Droplets are inject at $t = 50\tau_\ell$.

Method	k_{mean}/k_0	k_{std}/k_0	$\Delta k_{max}/\epsilon_0$	$\epsilon_{mean}/\epsilon_0$	$\epsilon_{std}/\epsilon_0$	$\Delta\epsilon_{max}/\epsilon_0$
Original SP constant-k from eq. (19)	0.998	0.0002	0.0020	0.993	0.0924	0.1924
Original TP constant-k from eq. (41)	0.999	0.0002	0.0014	0.893	0.1022	0.3578
Modified constant-k from eq. (57)	1.000	0.0000	0.0000	0.998	0.1050	0.2258
Original SP constant-ϵ from eq. (23)	1.117	0.1071	0.3805	1.058	0.0020	0.0637
Original TP constant-ϵ from eq. (46)	1.089	0.0444	0.1859	1.058	0.0019	0.0631
Modified constant-ϵ from eq. (58)	1.015	0.0812	0.2675	1.000	0.0001	0.0002
Original SP constant-$k\epsilon$ from eq. (27)	1.070	0.0583	0.1771	0.994	0.0523	0.1206
Original TP constant-$k\epsilon$ from eq. (48)	1.040	0.0558	0.1304	1.021	0.0564	0.1445
Modified constant-$k\epsilon$ from eq. (59)	1.033	0.0437	0.1288	0.972	0.0386	0.1025

TABLE IV: Mean, standard deviation and maximum oscillation amplitude of k and ϵ with respect to the linear forcing method for TPE test case taken from $t/\tau_\ell = 75$ to $t/\tau_\ell = 100$.

constant-ϵ by only looking at the figures. However, the statistical convergence shows improvement for both k and ϵ for the TPD case in table IV while it only improves the converged state for the TPE case in table V. In general, the modified form allows reducing the amplitude of oscillations and standard deviation, which demonstrates the capability of the proposed modification of the original forcing methods.

Method	k_{mean}/k_0	k_{std}/k_0	$\Delta k_{max}/\epsilon_0$	$\epsilon_{mean}/\epsilon_0$	$\epsilon_{std}/\epsilon_0$	$\Delta\epsilon_{max}/\epsilon_0$
Original SP constant-k from eq. (19)	0.999	0.0002	0.0014	0.978	0.0932	0.2472
Original TP constant-k from eq. (41)	0.999	0.0001	0.0011	1.027	0.0972	0.3066
Modified constant-k from eq. (57)	1.000	0.0000	0.0000	0.987	0.1147	0.2700
Original SP constant-ϵ from eq. (23)	1.032	0.0533	0.1754	1.009	0.0012	0.0133
Original TP constant-ϵ from eq. (46)	1.038	0.0787	0.2174	1.009	0.0011	0.0120
Modified constant-ϵ from eq. (58)	0.961	0.0891	0.2331	1.000	0.0000	0.0001
Original SP constant-$k\epsilon$ from eq. (27)	1.026	0.0546	0.1346	0.988	0.0492	0.0989
Original TP constant-$k\epsilon$ from eq. (48)	1.032	0.0460	0.1199	0.982	0.0435	0.0905
Modified constant-$k\epsilon$ from eq. (59)	1.002	0.0453	0.1060	1.002	0.0454	0.0921

TABLE V: Mean, standard deviation and maximum oscillation amplitude of k and ϵ with respect to the linear forcing method for TPD test case taken from $t/\tau_\ell = 75$ to $t/\tau_\ell = 100$.

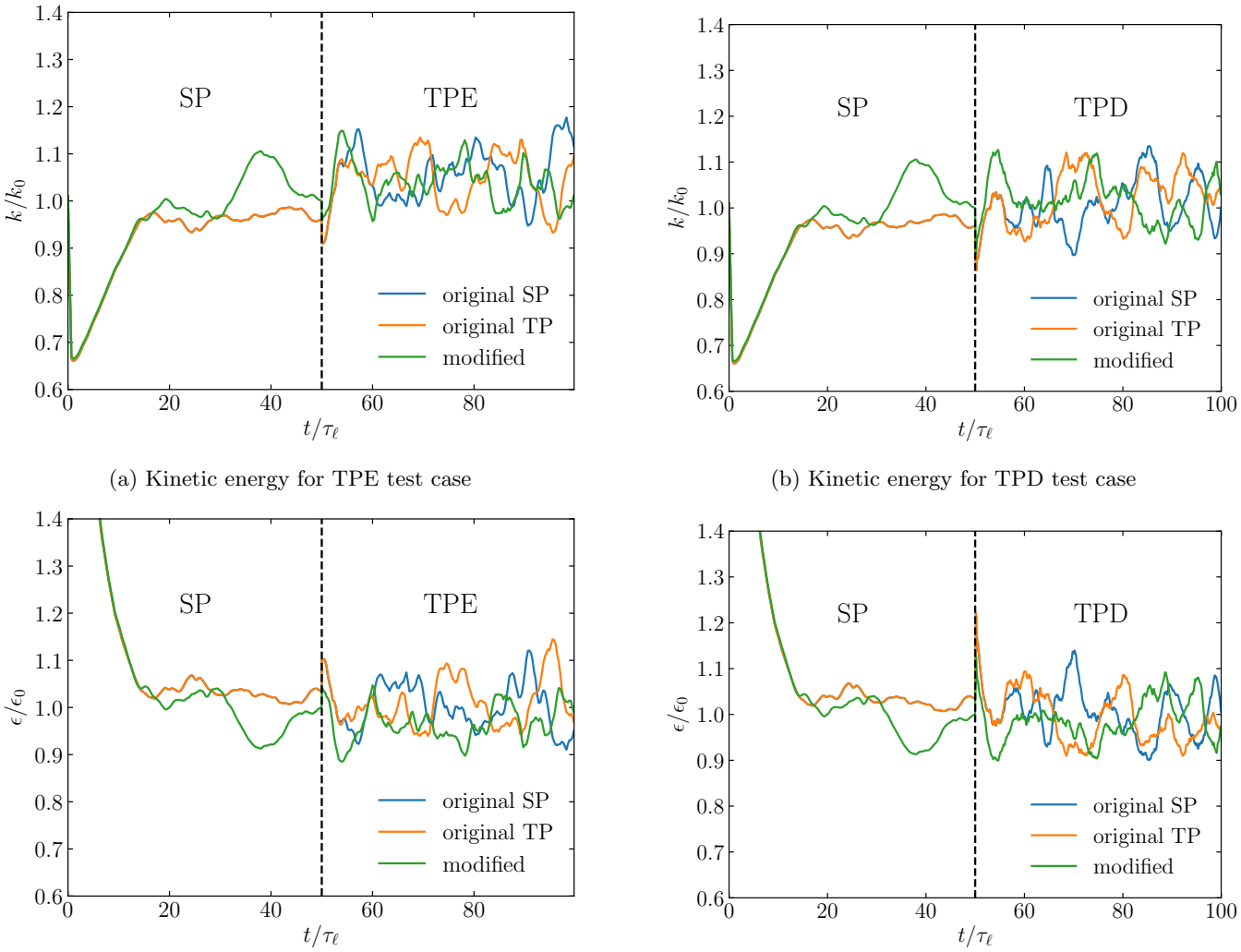

(a) Kinetic energy for TPE test case

(b) Kinetic energy for TPD test case

(c) Dissipation rate for TPE test case

(d) Dissipation rate for TPD test case

FIG. 9: Evolution of k for TPE (a) and TPD (b) test cases and ϵ for TPE (c) and TPD (d) test cases using the general constant-energetics methods based on the original form developed for single-phase flows (original SP) eq. (27), the original form extended to two-phase flows (original TP) eq. (59) and the modified form eq. (48).

C. Modulation of turbulence

With the growing interest in turbulent two-phase flows, our framework provides valuable insights and solutions to the control of turbulence, opening avenues for further exploration and refinement in understanding turbulent flows within the realm of two-phase processes. However, for the study of the modulation of turbulence by particles [44, 55], droplets [18] or bubbles [56], the forcing of turbulence in the physical space modifies the kinetic energy spectrum at all wavenumbers [57, 58]. The issue of forcing is then at the interpretation level: how can the contributions of turbulence forcing and particle forcing be discriminated in the energy transfer function? A solution has been proposed in [13] where turbulence is injected in a selected range of wavenumbers, making a clear separation between the energy transfer modulation due to the two-way coupling and the turbulence forcing. The main drawback of this approach is that it requires computing the forcing term in the spectral space, removing the benefits of using a linear forcing method. Another solution that only requires work in the spatial space is to apply an ABC flow which only injects turbulence at a given length scale [26]. This strategy has been applied successfully for the study of turbulent emulsions by [27].

VII. CONCLUSIONS AND FUTURE WORK

This paper introduces a general framework to address the challenges of forcing turbulence within single-phase and two-phase flows. Following a thorough examination of single-phase linear forcing techniques, we have established a constant-energetics forcing method that generalizes the constant-k, constant-ϵ and hybrid approach of Bassenne *et al.* [12]. A linear stability analysis allowed us to demonstrate the stability of this novel general constant-energetics forcing method for $0 < \chi < 1$. Our findings reveal an under-prescription of kinetic energy for all forcing methods except for constant-k forcing, which is related to numerical dissipation. Hence, we have tackled the unexplored challenge of numerical dissipation in two-phase flows, highlighting its origin and proposing modifications to constant-energetics forcing methods. This adaptation bridges the work of Duret *et al.* [29] and Bassenne *et al.* [12] to improve the constant-energetics methods in the presence of numerical dissipation. Finally, we validated a solution to prevent exponential kinetic energy growth due to capillary forces. The general constant-energetic forcing was then extended to two-phase flows using the same strategy as single-phase flows. It was also demonstrated that the modified approach introduced in this work was the most suited to control energetics when forcing turbulence in two-phase flows as proposed by Duret *et al.* [29].

Finally, the strategy developed here can also be extended to consider more complex flows such as magneto-hydrodynamics [59] or reactive flows [9]. Future research efforts should prioritize the refinement of techniques for controlling length scales, a crucial aspect constraining the development of numerical setups. Additionally, the development of anisotropic and inhomogeneous forcing will significantly expand the range of applicability of the linear forcing.

Appendix A: Impact of initial solution on statistics convergence

In this section, two initialization methodologies are compared to showcase the ability of the solver to converge to the prescribed turbulent flow. The first initialization takes a simple ABC [26] flow of the form:

$$\mathbf{u}^{ABC} = \begin{pmatrix} A[\cos(\kappa_f y) + \sin(\kappa_f z)] \\ A[\cos(\kappa_f z) + \sin(\kappa_f x)] \\ A[\cos(\kappa_f x) + \sin(\kappa_f y)] \end{pmatrix}, \tag{A1}$$

with $A = 1$ and $\kappa_f = 1$ by default.
The second initialization is based on a prescribed energy spectrum (PES) $E_0(\kappa)$ defined as in [10]:

$$E_0(\boldsymbol{\kappa}) = \frac{32}{3} k_0 \sqrt{\frac{2}{\pi}} \frac{\boldsymbol{\kappa}^4}{\kappa_0^5} \exp\left(-2\frac{\boldsymbol{\kappa}^2}{\kappa_0^2}\right), \tag{A2}$$

with $\kappa_0 = 2\pi/\ell$. Note that other energy spectrum forms can be prescribed which holds the same properties [18]. Then the spectral velocity $\hat{\mathbf{u}}(\boldsymbol{\kappa})$ is obtained by choosing random phases with the methodology described in [11] and is corrected to be divergence-free:

$$\hat{\mathbf{u}}(\boldsymbol{\kappa}) = \hat{\mathbf{u}}(\boldsymbol{\kappa}) - \boldsymbol{\kappa} \frac{\hat{\mathbf{u}}(\boldsymbol{\kappa}) \cdot \boldsymbol{\kappa}}{\boldsymbol{\kappa} \cdot \boldsymbol{\kappa}}. \tag{A3}$$

Finally, the initial velocity field $\mathbf{u}^{PES}$ is obtained from an inversed Fourier transform.

In fig. 10, the energy spectrum of both initializations is depicted to illustrate their differences. While the ABC flow contains all the energy at the prescribed wavenumber κ_f, the PES initialization already exhibits an energy cascade with the maximum energy at κ_0. It's worth noting that the ABC flow can be parameterized [26] to yield the correct initial kinetic energy k_0 and to drift the energy peak at the integral scale ℓ. An additional ABC flow $\mathbf{u}^{PABC}$ meeting these criteria has been added to the study with $A = u_0$ and $\kappa_f = \kappa_0$.

From the evolution of k and ϵ given in fig. 11, it is clear that all simulations lead to the same statistical convergence after a transient period of $30\tau_\ell$. The ABC initialization first shows a great rise of kinetic energy followed by a large dissipation rate to finally collapse and converge to the target turbulence. This numerical experiment proves that the linear forcing is not dependent of the initial solution at the steady state while the transient part is largely affected with a significant increase of the period length. A good practice is then to initialize with a good guess of the turbulent flow even if a simple prescribed ABC flow is enough to obtain quick convergence to the steady state. It is interesting for ease of implementation compared to the prescribed spectrum method which requires the use of an FFT library

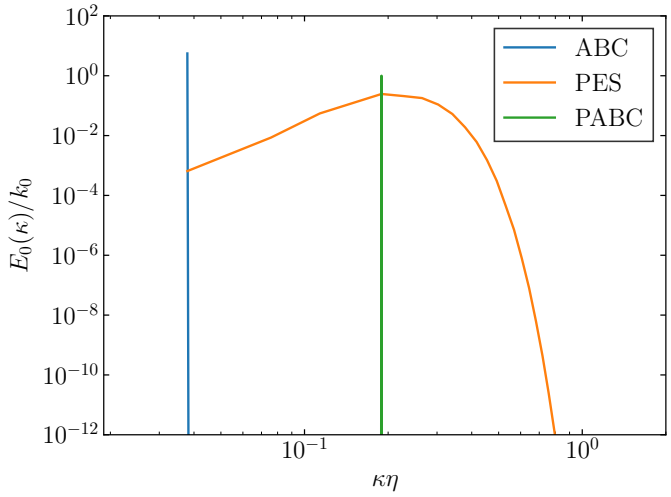

FIG. 10: Energy spectrum of the three initial velocity fields tested in this study.

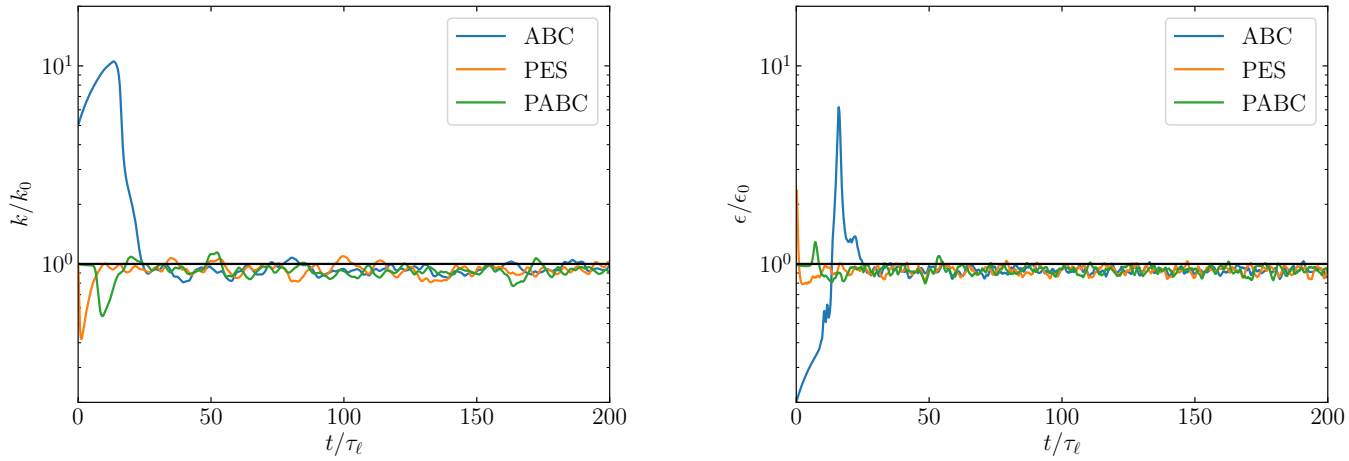

(a) (b)

FIG. 11: Evolution of k and ϵ for three initial solutions using the constant-$\mathcal{P}_T$ forcing. The y-axis is in log to better show the oscillations around the target values of k and ϵ.

which was initially undesired when using the linear forcing approach.

[1] H. R. Pruppacher and J. D. Klett, *Microphysics of clouds and precipitation* (Springer Science & Business Media, 2012).
[2] M. W. Schmeeckle, Journal of Geophysical Research: Earth Surface **119**, 1240 (2014).
[3] X. Hu, A. D. Ilgun, A. Passalacqua, R. O. Fox, F. Bertola, M. Milosevic, and F. Visscher, International Journal of Chemical Reactor Engineering **19**, 193 (2021).
[4] M. Arai, Engineering **5**, 519 (2019).
[5] T. S. Lundgren, Center for Turbulence Research Annual Research Briefs 2003 (2003).
[6] C. Rosales and C. Meneveau, Physics of fluids **17** (2005).
[7] A. Chouippe and M. Uhlmann, Physics of Fluids **27** (2015).
[8] S. Lapointe, B. Savard, and G. Blanquart, Combustion and flame **162**, 3341 (2015).
[9] M. Klein, N. Chakraborty, and S. Ketterl, Flow, Turbulence and Combustion **99**, 955 (2017).
[10] P. L. Carroll and G. Blanquart, Physics of Fluids **25** (2013).
[11] V. Eswaran and S. B. Pope, Computers & Fluids **16**, 257 (1988).
[12] M. Bassenne, J. Urzay, G. I. Park, and P. Moin, Physics of Fluids **28** (2016).

[13] G. Mallouppas, W. George, and B. van Wachem, Physics of Fluids **25** (2013).
[14] A. Begemann, T. Trummler, E. Trautner, J. Hasslberger, and M. Klein, The Canadian Journal of Chemical Engineering **100**, 3548 (2022).
[15] B. De Laage de Meux, B. Audebert, R. Manceau, and R. Perrin, Physics of Fluids **27** (2015).
[16] S. Ketterl and M. Klein, Flow, Turbulence and Combustion **101**, 413 (2018).
[17] J. A. Palmore Jr and O. Desjardins, Physical Review Fluids **3**, 034605 (2018).
[18] M. S. Dodd and A. Ferrante, Journal of Fluid Mechanics **806**, 356 (2016).
[19] O. Desjardins, G. Blanquart, G. Balarac, and H. Pitsch, Journal of Computational Physics **227**, 7125 (2008).
[20] S. Mirjalili and A. Mani, Journal of Computational Physics **426**, 109918 (2021).
[21] S. Popinet, Journal of Computational Physics **228**, 5838 (2009).
[22] K. Eisenschmidt, M. Ertl, H. Gomaa, C. Kieffer-Roth, C. Meister, P. Rauschenberger, M. Reitzle, K. Schlottke, and B. Weigand, Applied Mathematics and Computation **272**, 508 (2016).
[23] W. Aniszewski, T. Arrufat, M. Crialesi-Esposito, S. Dabiri, D. Fuster, Y. Ling, J. Lu, L. Malan, S. Pal, R. Scardovelli, *et al.*, Computer Physics Communications **263**, 107849 (2021).
[24] V. Boniou, T. Schmitt, and A. Vié, International Journal of Multiphase Flow **149**, 103957 (2022).
[25] M. Crialesi-Esposito, N. Scapin, A. D. Demou, M. E. Rosti, P. Costa, F. Spiga, and L. Brandt, Computer Physics Communications **284**, 108602 (2023).
[26] P. Mininni, A. Alexakis, and A. Pouquet, Physical Review E **74**, 016303 (2006).
[27] M. Crialesi-Esposito, M. E. Rosti, S. Chibbaro, and L. Brandt, Journal of Fluid Mechanics **940**, A19 (2022).
[28] Y. Yao and J. Capecelatro, Journal of Fluid Mechanics **911**, A10 (2021).
[29] B. Duret, G. Luret, J. Reveillon, T. Ménard, A. Berlemont, and F.-X. Demoulin, International Journal of Multiphase Flow **40**, 93 (2012).
[30] J. U. Brackbill, D. B. Kothe, and C. Zemach, Journal of computational physics **100**, 335 (1992).
[31] J. B. Bell, P. Colella, and H. M. Glaz, Journal of computational physics **85**, 257 (1989).
[32] C. W. Hirt and B. D. Nichols, Journal of computational physics **39**, 201 (1981).
[33] W. J. Rider and D. B. Kothe, Journal of computational physics **141**, 112 (1998).
[34] M. M. Francois, S. J. Cummins, E. D. Dendy, D. B. Kothe, J. M. Sicilian, and M. W. Williams, Journal of Computational Physics **213**, 141 (2006).
[35] J. Jeong and F. Hussain, Journal of fluid mechanics **285**, 69 (1995).
[36] R. Boukharfane, A. Er-Raiy, M. Parsani, and N. Chakraborty, Scientific reports **11**, 15242 (2021).
[37] S. Mukherjee, A. Safdari, O. Shardt, S. Kenjereš, and H. E. Van den Akker, Journal of Fluid Mechanics **878**, 221 (2019).
[38] M. Crialesi-Esposito, S. Chibbaro, and L. Brandt, Communications Physics **6**, 5 (2023).
[39] A. Ten Cate, J. J. Derksen, L. M. Portela, and H. E. Van Den Akker, Journal of Fluid Mechanics **519**, 233 (2004).
[40] M. Uhlmann and A. Chouippe, Journal of fluid mechanics **812**, 991 (2017).
[41] J. O. Hinze, AIChE journal **1**, 289 (1955).
[42] M. C. Naru, *Numerical simulation of a water/oil emulsion in a multiscale/multiphysics context*, Theses, Sorbonne Université (2021).
[43] N. Fintzi, J.-L. Pierson, and S. Popinet, Acta Mechanica (to be submitted) (2024).
[44] A. Ferrante and S. Elghobashi, Physics of fluids **15**, 315 (2003).
[45] E. Tangermann and M. Klein, Fluids **5**, 130 (2020).
[46] S. Pope, *Turbulent Flows* (Cambridge University Press, 2000).
[47] V. Le Chenadec and H. Pitsch, Journal of Computational Physics **249**, 185 (2013).
[48] M. Rudman, International Journal for numerical methods in fluids **28**, 357 (1998).
[49] O. Desjardins and V. Moureau, Center for Turbulent Research, Summer Programm **2010**, 313 (2010).
[50] F. S. Schranner, J. A. Domaradzki, S. Hickel, and N. A. Adams, Computers & Fluids **114**, 84 (2015).
[51] A. Naso and A. Prosperetti, New Journal of Physics **12**, 033040 (2010).
[52] A. Loisy and A. Naso, Physical Review Fluids **2**, 014606 (2017).
[53] S. Popinet, Annual Review of Fluid Mechanics **50**, 49 (2018).
[54] M. O. Abu-Al-Saud, S. Popinet, and H. A. Tchelepi, Journal of Computational Physics **371**, 896 (2018).
[55] R. Letournel, F. Laurent, M. Massot, and A. Vié, International Journal of Multiphase Flow **125**, 103233 (2020).
[56] I. M. Mazzitelli, D. Lohse, and F. Toschi, Journal of Fluid Mechanics **488**, 283 (2003).
[57] F. Lucci, A. Ferrante, and S. Elghobashi, Journal of Fluid Mechanics **650**, 5 (2010).
[58] S. Elghobashi, Annual Review of Fluid Mechanics **51**, 217 (2019).
[59] A. Chernyshov, K. Karelsky, and A. Petrosyan, Physics of Plasmas **17** (2010).